Published in final edited form as:
Cancer Res. 2021 August 15; 81(16): 4242–4256. doi:10.1158/0008-5472.CAN-21-1677.

MYC and MIZ1-dependent vesicular transport of double-strand RNA controls immune evasion in pancreatic ductal adenocarcinoma

Bastian Krenz[#1], **Anneli Gebhardt-Wolf**[#1], **Carsten P. Ade**[1], **Abdallah Gaballa**[1], **Florian Roehrig**[2], **Emilia Vendelova**[3], **Apoorva Baluapuri**[4], **Ursula Eilers**[5], **Peter Gallant**[1], **Luana D'Artista**[6], **Armin Wiegering**[1,7], **Georg Gasteiger**[3], **Mathias T. Rosenfeldt**[8], **Stefan Bauer**[9], **Lars Zender**[6], **Elmar Wolf**[4], **Martin Eilers**[1]

[1]Theodor Boveri Institute, Department of Biochemistry and Molecular Biology, Biocenter, University of Würzburg, 97074 Würzburg, Germany

[2]Comprehensive Cancer Center Mainfranken, Core Unit Bioinformatics, Biocenter, University of Würzburg, 97074 Würzburg, Germany

[3]Institute of Systems Immunology, University of Würzburg, 97078 Würzburg, Germany

[4]Cancer Systems Biology Group, Department of Biochemistry and Molecular Biology, Biocenter, University of Würzburg, 97074 Würzburg, Germany

[5]Core Unit High-Content Microscopy, Biocenter, University of Würzburg, 97074 Würzburg, Germany

[6]Department of Medical Oncology and Pneumology (Internal Medicine VIII), University Hospital Tübingen, 72076 Tübingen, Germany

[7]Department of General, Visceral, Transplant, Vascular and Pediatric Surgery, University Hospital Würzburg, 97080 Würzburg, Germany

[8]Institute for Pathology, University of Würzburg, 97080 Würzburg, Germany

[9]Institute for Immunology, BMFZ, Philipps-University of Marburg, 35043 Marburg, Germany

[#] These authors contributed equally to this work.

Abstract

Deregulated expression of the MYC oncoprotein enables tumor cells to evade immune surveillance, but the mechanisms underlying this surveillance are poorly understood. We show here that endogenous MYC protects pancreatic ductal adenocarcinoma driven by $KRAS^{G12D}$ and $TP53^{R172H}$ from eradication by the immune system. Deletion of TANK-Binding Kinase 1 (TBK1) bypassed the requirement for high MYC expression. TBK1 was active due to the accumulation

Correspondence to: Martin Eilers.

Corresponding Author: Martin Eilers, Biocenter, Theodor Boveri Institute, Department of Biochemistry and Molecular Biology, Biocenter, University of Würzburg, 97074 Würzburg, Germany, martin.eilers@biozentrum.uni-wuerzburg.de Phone: +49 931 31 84112.

Conflicts of Interest:
The authors do not declare a conflict of interest.

Europe PMC Funders Author Manuscripts

of double-stranded RNA (dsRNA), which was derived from inverted repetitive elements localized in introns of nuclear genes. Nuclear-derived dsRNA is packaged into extracellular vesicles and subsequently recognized by toll-like receptor 3 (TLR3) to activate TBK1 and downstream MHC class I expression in an autocrine or paracrine manner before being degraded in lysosomes. MYC suppressed loading of dsRNA onto TLR3 and its subsequent degradation via association with MIZ1. Collectively, these findings suggest that MYC and MIZ1 suppress a surveillance pathway that signals perturbances in mRNA processing to the immune system, which facilitates immune evasion in pancreatic ductal adenocarcinoma (160 words).

Keywords

MYC; PDAC; MIZ1; dsRNA; TBK1; NF-κB; toll-like receptor 3

Introduction

Deregulated expression of the *MYC* proto-oncogene or one of its paralogues, *MYCN* and *MYCL*, drive tumorigenesis in a wide range of tissues (1). MYC proteins bind to the vast majority of all active promoters and exert widespread effects on the function and composition of the transcription machinery (1,2). While MYC proteins broadly stimulate gene expression, they also suppress NF-κB-dependent pro-inflammatory and IRF-dependent antiviral gene expression in multiple experimental systems (3,4). Consistent with the latter observations, recent work has uncovered a potent ability of MYC to enable tumor cells to escape recognition and elimination by the immune system (3,5,6). For example, T cell lymphomas driven by a doxycycline-inducible MYC transgene are eliminated in a T and NK cell-dependent manner when MYC expression is switched off (6,7) and reversion of the activity of a MYCER transgene leads to an immune cell-mediated regression in models of lung and pancreatic ductal adenocarcinoma (PDAC) (5). MYC-mediated immune escape correlates closely with the suppression of genes encoding MHC class I antigens and pro-inflammatory cytokines (4).

NF-κB and IRFs are activated by a broad spectrum of stress signals (8). These include signaling cascades that sense aberrant nucleic acid species via pattern recognition receptors (PRRs), which either recognize cytosolic DNA, such as the AIM and the STING receptors, or double-stranded RNA (dsRNA), such as MDA5, toll-like receptor 3 (TLR3) and the RIG-I receptors (9). PRRs have critical roles during infection (10) but also recognize self-nucleic acids: a paradigm example is the sensing of cytosolic self-DNA that is released from the nucleus in response to DNA damage (11). These mechanisms enable cells to sense genomic instability (12) and mitochondrial disfunction (13) and signal perturbances to the immune system.

The *Myc* gene is haplo-insufficient for tumorigenesis in mouse models of PDAC driven by mutant KRAS, and depletion of MYC or expression of a dominant-negative allele of MYC in established tumors leads to tumor regression (14–16). One mechanism how MYC suppresses transcription is via association with MIZ1 (17) and, like *Myc*, *Miz1* is haplo-insufficient for pancreatic tumorigenesis. MIZ1 binds to and regulates a stereotypic set of

Europe PMC Funders Author Manuscripts

genes involved in vesicle biogenesis and transport and is required, for example, for vesicle flux during autophagy (18). Whether this function relates to the immune-evasive effects of MYC is unknown. Here we show that MYC and MIZ1 control the vesicular transport of dsRNA derived from the introns of nuclear genes and that this pathway controls MHC class I expression linking it directly to the immune-suppressive functions of deregulated MYC.

Materials and Methods

Mouse experiments

All animal procedures were approved by the Regierung von Unterfranken under protocol numbers RUF 55.2-2532-2-148 and RUF 55.2.2-2532.2-1026. For orthotopic transplantation, mice (C57BL/6J, RRID:IMSR_JAX:000664; NOD.Cg-*Rag1*^{tm1Mom} *Il2rg*^{tm1Wjl}/SzJ (NRG), RRID:IMSR_JAX:007799; BALB/cAnNRj-Foxn1 nu/nu mice (nude), Janvier LABS; B6.129S7-Rag1tm1Mom/J (Rag1-/-), RRID:IMSR_JAX:002216) were anaesthetized, the spleen and the pancreas were externalized and 50,000 modified KPC cells were injected in 50 μL Matrigel / PBS (2:1) into the pancreatic tail. Luciferase activity was measured with an IVIS camera. For histology, the following antibodies were used: α-CD3 (SP7, Abcam, 1:100, RRID: AB_443425), α-CD4 (4SM95, ebioscience, 1:100, RRID: AB_2573008), α-CD8 (Thermo scientific, 1:100, RRID: AB_149750), α-F4/80 (CI:A3-1, Abcam, 1:1,000, RRID: AB_1140040), α-NKp46/NCR1 (R&D systems, RRID: AB_355192).

Cell culture and flow cytometric analysis

HEK293TN (RRID:CVCL_UL49), PANC1 (RRID:CVCL_0480), PaTu 8988T (RRID:CVCL_1847), KPC and U2OS (RRID:CVCL_0042) cells were cultured in DMEM (Sigma-Aldrich) and ASPC1 (RRID:CVCL_0152), MZ1, Dan-G (RRID:CVCL_0243), IMIM RC1 and Panc0813 (RRID:CVCL_1638) in RPMI (Sigma-Aldrich) supplemented with 10% fetal calf serum (Biochrom) and 1% penicillin-streptomycin (Sigma-Aldrich). Human PDAC cells were provided by Matthias Rosenfeldt (2020), KPC cells from Jens Sieveke (2014). HEK293TN and U2OS cells were obtained from ATCC. Human Cells were verified by short tandem repeat profiling, Cells were regularly tested for mycoplasma contamination using standard methods (Arbeitsgemeinschaft Gentechnik, AM029). The latest tests were in September 2020. For staining of MHC class I proteins, we used H-2Db (Invitrogen, RRID:AB_2539376) and H-2kb (Bio C Cell, RRID: AB_10949300) antibodies. The measurement was performed using BD FACSCanto II flow cytometry and BD FACSDIVA software (RRID:SCR_001456).

Immunoblot and Immunofluorescence

The following primary antibodies were used: Vinculin (V9131, Sigma Aldrich, 1:3,000, RRID: AB_477629), MYC (Y69, Abcam, 1:1,000, RRID: AB_731658), TBK1 (D1B4, Cell signaling, 1:1,000, RRID: AB_2255663), P-TBK1 (S172, D52C5, Cell signaling, 1:1,000, RRID: AB_10693472), IKBA (L35A5, 1:2,000, Cell signaling, RRID: AB_390781), P-IKBA (14D4, 1:2,000, Cell signaling, RRID: AB_561111), P62 (MBL, 1:1,000, RRID: AB_1279301), LC3 (MBL, 1:1,000, RRID: AB_2274121), P-P62 (S403, Thermo Fisher Scientific, 1:1,000, RRID: AB_2736424), TLR3 (Abcam, 1:1,000, RRID: AB_956368),

Actin (Sigma-Aldrich, 1:10,000, RRID: AB_476744), J2 (Kerafast/Scicons), ssDNA (Millipore, RRID: AB_570342), H3K9me3 (Active Motif, RRID: AB_2532132), anti-BrdU (Cell signaling, RRID: AB_10548898), Tubulin (Santa Cruz, RRID: AB_2241125).

fCLIP and sequencing of double-stranded RNA

fCLIP was adapted from (19) and dsRNA sequencing was performed as described in (20).

Isolation of extracellular vesicles

For purification of extracellular vesicles, KPC cells were incubated in 150 mm culture plates over night to allow attachment of cells. Medium was exchanged and cells were treated for 48 h. Conditioned medium was collected and centrifuged at 1,500 rpm for 10 min at 4 °C and subsequently filtered through a 0.2 μM filter. To disrupt extracellular vesicles in respective samples 1% Triton was added and incubated at 4 °C for 10 min. Supernatant was transferred to ultracentrifugation tubes and ultra-centrifuged with a Beckmann SW32Ti rotor at 30,000 rpm for 90 min at 4 °C. The pellet was washed with cold PBS and re-centrifuged. The pellet was dissolved in PBS or in full RPMI medium if used for stimulation of bone marrow derived dendritic cells (BMDCs). BMDCs were generated from bone marrow cells of C57BL/6 mice. 1 million BMDCs were plated in 48 well-plates (Nunc, Roskilde, Denmark) in complete RPMI medium. Control BMDCs were treated in similar way without exposure to extracellular vesicles.

Results

MYC is required for the rapid growth of KPC cells in culture

In human PDAC, both copy number gains (21) and elevated mRNA levels of MYC (Supplementary Figure S1A) predict poor survival. To analyze the role of endogenous MYC in the growth of PDAC cells, we used a tumor cell line that has been established from the “KPC” mouse model (22). In this model, the concomitant expression of $TP53^{R172H}$ and $KRAS^{G12D}$ is induced in pancreatic progenitor cells via Cre-mediated recombination. To ensure efficient depletion of MYC, cells were stably infected with two different doxycycline-inducible shRNAs targeting the *MYC* mRNA and infected cells were selected and used for subsequent analyses. Addition of doxycycline to these cells led to a robust reduction in MYC protein levels (Figure 1A). Depletion of MYC caused multiple phenotypes that are expected from published work. Most notably, the proliferation rate as measured as an increase in cell number strongly depended on MYC (Figure 1B). Consistently, depletion of MYC caused a decrease in the percentage of cells incorporating BrdU (Supplementary Figure S1B). Combining the cell cycle analysis with the population doubling time showed that depletion of MYC prolonged all phases of the cell cycle (Figure 1C,D). The decrease in proliferation was not due to senescence, since there was no increase in the percentage of cells staining positive for H3K9me3, a marker of senescent cells (Supplementary Figure S1C). In contrast, cells underwent senescence in response to the CDK4/6 inhibitor Palbociclib (Palb), as expected from the literature. KPC cells underwent morphological changes upon depletion of MYC and showed a flattened morphology and increased in apparent cell size when MYC was depleted (Supplementary Figure S1D). To confirm these findings and ensure that they were not due to the expression of shRNAs,

we established a second model, in which we used CRISPR/Cas9 to disrupt the endogenous MYC gene after stably expressing a doxycycline-inducible human MYC transgene (Figure 1A and Supplementary Figure S1E). These cells recapitulated the phenotypes described above and showed, for example, a strongly doxycycline-regulated proliferation (Figure 1B).

To understand the dependence of cell proliferation on endogenous MYC, we performed RNA sequencing experiments from cultured cells upon doxycycline induced depletion of MYC for 48 h. In order to ensure that changes in gene expression also occur *in vivo*, we orthotopically transplanted cells into syngeneic mice and let tumors grow for seven days before doxycycline-containing food was added for 48 h. Both in tissue culture and *in vivo*, depletion of MYC caused a decrease in expression of multiple canonical gene sets of MYC target genes, including the “hallmark” MYC target gene sets that have been compiled from multiple individual gene expression analyses (Figure 1E). GO term analysis showed that these sets include multiple genes encoding proteins associated with canonical functions of MYC, such as ribosome biogenesis, rRNA processing and mRNA translation, RNA splicing and mRNA processing (Supplementary Figure S1F). Depletion of MYC also led to a strong increase in expression of gene sets that have previously been identified as targets for repression by MYC. Specifically, genes of the TGF-β pathway, target genes of NF-κB (which are largely identical to the “inflammatory response” gene set) and IL6/STAT3-dependent genes were up-regulated in response to MYC depletion (Figure 1E). IL6/JAK/STAT3-dependent genes may be induced indirectly since IL6 is a target gene of NF-κB (8). We did not observe a consistent regulation of interferon-dependent genes in these cells (see Discussion). Chromatin binding data from the same cellular system showed that both MYC and MIZ1 are virtually absent from the promoters of NF-κB dependent genes when compared with both MYC-activated and unregulated genes (Figure 1F, Supplementary Figure 1G,H), arguing that the effects of MYC-on NF-κB-dependent genes are largely indirect.

Immune-mediated tumor regression upon MYC depletion in vivo

In order to understand how the MYC-dependent effects on gene expression translate into *in vivo* growth behavior, we initially transplanted KPC cells expressing luciferase and doxycycline-inducible shRNAs targeting *MYC* into syngeneic mice and let tumors grow for seven days before addition of doxycycline to the food. Similar to human PDAC the tumor cells formed irregular, duct-like, glandular structures, grew in sheets or were individually dispersed, and elicited a stromal response (Supplementary Figure S2A). Addition of doxycycline for two weeks had no effect on the growth of tumors expressing a control shRNA (Figure 2A). In contrast, doxycycline led to tumor regression in mice expressing shRNAs targeting *MYC* (Figure 2B). This correlated with an extension of the median lifespan from 29 days to 70 days upon depletion of MYC (Figure 2C, $p<0.0001$, Mantel-Cox test). RNA sequencing of tumors at endpoint that had regrown in the presence of doxycycline showed that both the reduction in expression of MYC-activated genes and the increase in MYC-repressed genes had largely reverted (Supplementary Figure S2B). This correlated with a reduction in shRNA-mediated MYC depletion and an adaptation of the network of MAX-interacting proteins (Supplementary Figure S2C). These findings suggested that escaping tumors restore MYC function and limited the analysis of the effects

of MYC depletion on long-term survival. To confirm these observations, we engineered KPC cells with a doxycycline-inducible *MYC* gene on the background of a deletion of the endogenous *MYC* gene and transplanted them into immunocompetent mice. We observed a similar dependence of the median lifespan on MYC levels (+ MYC median lifespan: 21 days; - MYC median lifespan: 47 days; p=0.0002, Mantel-Cox test) (Figure 2D and Supplementary Figure S2D).

Tumor regression upon depletion of MYC was paralleled by weak increases in the number of $CD3^+$, $CD4^+$ and $CD8^+$ T cells (Supplementary Figure 3A). We also observed a variable influx of B cells (B220) into the tumor tissue, while the number of macrophages did not alter upon MYC depletion (Supplementary Figure S3A,B). NK cells were rarely found in the tumor tissue (Supplementary Figure S3C). To test the relevance of these changes for tumor regression, we transplanted the KPC cells expressing shRNAs targeting *MYC* into different immune-compromised mice strains: Upon transplantation into NRG mice, which lack functional T and B lymphocytes as well as natural killer (NK) cells (23), engrafted tumors show a similar histology as described before (Supplementary Figure S3D). Under identical experimental conditions, depletion of MYC caused a moderate decrease in tumor growth, rather than tumor regression (Figures 2E,F). Similarly, no tumor regression was observed upon depletion of MYC in cells that had been transplanted into nude mice, which lack T cells, and into RAG1-deficient mice, which lack both B and T cells, although the decreases in tumor growth were more pronounced than in NRG mice (Figure 2F). Correspondingly, survival of nude and RAG1-deficient mice was identical to control mice in the presence of MYC, but significantly shorter when MYC was depleted (Supplementary Figure S3E). The data argue that T cells are required for tumor elimination and that several types of immune cells conspire to eliminate tumors upon MYC depletion. The weak effect of MYC depletion on tumor growth in immunodeficient mice was surprising in light of the strong dependence of cell growth on MYC in tissue culture. To understand this difference, we used the luciferase counts to estimate doubling times for KPC cells *in vivo*. This showed that the growth of tumors *in vivo* in the presence of MYC occurred much more slowly than in culture and was even slower than the growth observed in culture in the absence of MYC (Figure 2G). This correlated with a significant downregulation of gene sets encoding cell cycle genes *in vivo* relative to cells grown in culture and a corresponding upregulation of gene sets reflecting the interaction of tumor cells with their environment (Figure 2H). Collectively, the data show that MYC is required *in vivo* mainly to prevent an immune cell-mediated elimination of KPC tumors.

Activation of TBK1 is critical for tumor regression upon MYC depletion

Depletion of MYC induced pro-inflammatory and NF-κB-dependent gene expression both in tissue culture and *in vivo*, arguing that the induction does not depend on the tumor microenvironment. To identify the upstream signals that may drive this gene expression program, we surveyed the activity status of kinases that have been implicated in activation of NF-κB-dependent gene expression. These experiments revealed that TBK1 was rapidly activated, as documented by an increase in autophosphorylation at serine 172, in response to MYC depletion (Figure 3A,B). They also revealed a weaker, but consistent, increase in phosphorylation of IκBα at serine 32, indicating an increase in the activity of the IKKα

and/or IKKβ kinases (Supplementary Figure S4A). In contrast, the activity of IKKε, a kinase that is also implicated in NF-κB activation, decreased in response to MYC depletion (Supplementary Figure S4B), The increase in TBK1 activity was transient and declined three to six days after MYC depletion (Figure 3A,B). To test whether the activation of TBK1 is required for tumor regression upon MYC depletion, we deleted the *Tbk1* gene using specific guide RNAs. Immunoblots confirmed that the resulting KPC cells did not express any TBK1 (Figure 3C). Deletion of TBK1 had no measurable effects on the growth of KPC cells in culture, both in the absence or presence of MYC (Supplementary Figure S4C). *In vivo*, TBK1-deficient cells showed a tumor growth equal to that of control cells in the presence of MYC (Figure 3D). In contrast, deletion of TBK1 abrogated tumor regression and significantly shortened the survival of mice upon depletion of MYC (Figure 3D,E and Supplementary Figure S4D,E). Comparisons showed that tumor growth of TBK1-deleted cells in the absence of MYC was similar to that seen upon transplantation of TBK1 wildtype cells in RAG1-deficient mice in the absence of MYC (Supplementary Figure S4D), arguing that suppression of TBK1 activity is the major oncogenic activity of MYC in this experimental setting.

TBK1 is activated downstream of dsRNA originating from the nucleus

TBK1, IKKα and IKKβ take part in signaling pathways downstream of pattern recognition receptors that recognize unusual nucleic acid species, such as double-stranded RNA and single-stranded DNA. Immunofluorescence experiments using J2, a monoclonal antibody that detects double-stranded RNA, yielded a strong, MYC-dependent signal in the cytosol of KPC cells (Figure 4A,B) (24). Incubation of cells with RNase III, which degrades dsRNA, decreased the fluorescence, whereas incubation with RNase T1, which degrades single-stranded RNA, did not alter the signal, confirming the specificity of the signal (Figure 4B and Supplementary Figure S5A). Doxycycline-induced depletion of MYC strongly decreased the J2 immunofluorescence signal. Conversely, induction of MYC in KPC cells that have a knockout of endogenous MYC led to a time-dependent increase in J2 immunofluorescence (Supplementary Figure S5B). We also noted that the residual dsRNA after MYC-depletion transiently accumulated in a perinuclear region (Supplementary Figure S5C). Pre-incubation of cells for 24 h with inhibitors of kinases that block transcription by RNAPII, including 5,6-dichloro-1-β-D-ribofuranosyl-benzimidazole (DRB), LDC 0000 67, a specific CDK9 kinase inhibitor, and THZ1, a specific CDK7 kinase inhibitor, decreased the immunofluorescence signal to a similar extent as depletion of MYC (Figure 4C). Collectively, the data show that high levels of MYC lead to a RNAPII-dependent accumulation of dsRNA. Staining of KPC cells with an antibody that specifically recognizes single-stranded DNA (TNT-3) also yielded a positive signal in the cytosol, which was sensitive to pre-incubation of cells with the single-strand specific nuclease S1, but the signal intensity was heterogeneous between cells and the effect of MYC depletion was weak (Supplementary Figure S5D).

To identify the origin of dsRNA, we processed J2 immunoprecipitates from KPC cells spiked with lysates of human U2OS cells for next-generation sequencing. Controls consisting of immunoprecipitates of non-specific IgG and samples treated with RNase III were used to confirm the specificity of the sequencing results. These experiments showed

that there are two major sources of dsRNA (Figure 4D). One source is mitochondrial RNA, which arises since the mitochondrial genome is transcribed in a bidirectional manner (20) (Supplementary Figure S6A). The effect of MYC on mitochondrial transcription is most likely indirect, since multiple previous papers have noted that MYC promotes mitochondrial biogenesis and directly stimulates expression of the gene encoding the major mitochondrial transcription factor, TFAM, and many other nuclear encoded mitochondrial genes (25). The second source of dsRNA are repetitive elements located in nuclear genes (Figure 4D).

Mammalian cells have three major pattern recognition receptors (PRRs) that recognize dsRNA: RIG-I, MDA5 and TLR3 (10). The bulk of dsRNA that we sequenced had a length between 100 to 300 nucleotides and is therefore capable of activating the TLR3 and the RIG-I PRRs (26,27) (Figure 4E). To determine which cellular PRR binds dsRNA, we initially performed proximity ligation assays (PLA) using J2 and antibodies specific for each of these receptors, which showed that all three receptors are occupied by dsRNA in KPC cells, with signals for TLR3 being the strongest (Supplementary Figure S6B). Immunoprecipitation experiments coupled with RQ-PCR revealed that dsRNA was almost exclusively bound to TLR3 and that the amount of dsRNA bound to TLR3 was significantly enriched for nuclear-derived dsRNA relative to mitochondria-derived dsRNA as determined using a number of different primers (Figure 4F). To test whether TLR3 is required for activation of TBK1 upon depletion of MYC, we deleted *Tlr3* using two independent guide RNAs and found that phosphorylation of TBK1 at serine 172 is markedly decreased in TLR3 deleted cells upon MYC depletion using sgRNA #1 (Figure 4G,H). This was confirmed with a second sgRNA targeting *Tlr3*, which caused similar, albeit somewhat weaker effects. (Figure 4H). Furthermore, incubation of KPC cells with an TLR3/dsRNA complex inhibitor (28) abrogated activation of TBK1 upon MYC depletion (Figure 4I). Similarly, human tumor cells contain dsRNA originating from Alu elements localized in the intron of transcribed genes (Supplementary Figure S6C) and TLR3 binds this dsRNA in several different human PDAC cell lines (Figure 4J). We concluded that TBK1 is activated downstream of dsRNA that mainly originates in the nucleus; this observation is surprising, since TLR3 recognizes dsRNA in endosomes, not in the cytosol (29). We therefore decided to further characterize the source and the metabolism of dsRNA.

Nuclear dsRNA is derived from long and AT-rich introns

91% of the reads from the sequencing of the J2 immunoprecipitates representing nuclear dsRNA were derived from repetitive elements, with the B2 (24%) and B1 (14%) classes being predominant (Figure 5A). We noted a number of characteristic features of these dsRNA molecules: First, most reads representing B1 and B2 elements originate from the introns of a small number of host genes (n=64) (Figure 5B). Second, these host genes contain inverted repetitive elements, arguing that dsRNA synthesis does not depend on antisense transcription (Figure 5C). Third, dsRNA host genes were expressed at comparable levels to the median gene expression of all genes (Figure 5D) and their expression levels were unaffected by MYC (Figure 5E). Specifically, sequencing of nascent RNA harvested from cells either directly after a pulse of 4-thiouridine or after a pulse followed by a chase of 60 or 120 minutes showed that neither the synthesis nor the early processing of the 60 host introns of dsRNA were affected by MYC (Figure 5F). Furthermore, host

genes did not encode a functionally distinct class of proteins and are also not obviously co-regulated in response to another known stimulus. Intriguingly, host genes showed particularly long introns (Figure 5G), suggesting that the delay in completion of splicing opens a time window for the hybridization of inverted repeats that leads to dsRNA formation. Furthermore, host genes were AT-rich, raising the possibility that the editing of adenosine residues to inosine, which antagonizes dsRNA formation, is limiting on these genes (Figure 5H) (30). The data argue that nuclear-derived dsRNA originates from intronic RNA that escapes degradation.

MYC and MIZ1 control trafficking of intron-derived dsRNA

To understand how MYC controls levels of intron-derived dsRNA, we reanalyzed the RNA sequencing experiments described earlier and found that multiple genes encoding proteins involved in vesicular transport were up-regulated upon MYC depletion (Figure 6A). We have demonstrated previously that MYC can repress transcription via MIZ1 and that MIZ1 binds directly to multiple promoters of genes involved in vesicular transport and is required for multiple steps of intracellular vesicle transport, including autophagy (18). We confirmed that MYC associates with MIZ1 in PDAC cells (Figure 6B and Supplementary Figure S7A). Consistent with a model in which MYC antagonizes MIZ1 function, high levels of ZBTB17 gene expression (MIZ1) predict good prognosis in human PDAC patients (Supplementary Figure S7B). Furthermore, we used available ChIP sequencing data from cells expressing either wild-type MYC or MYCV394D (MYCVD), a point mutant allele that is deficient in binding to MIZ1, to show that both MYC and MIZ1 bind to the promoters of multiple genes involved in vesicle transport and stabilize each other's binding to these promoters (Supplementary Figure 7C,D). To test whether MYC represses genes involved in vesicular transport via MIZ1, we generated KPC cells in which addition of doxycycline leads to a knock-down of endogenous MYC as well as to an expression of either wild-type MYC or MYCVD (Supplementary Figure S7E). RNA sequencing of these cells showed that multiple genes encoding proteins involved in vesicular transport were up-regulated upon MYC depletion in a MIZ1-dependent manner, and that both gene sets encoding for proteins involved in secretion as well as in endocytosis and autophagosome formation were affected (Figure 6A). These findings raised the possibility that MYC controls the trafficking of intron-derived dsRNA via association with MIZ1.

To probe whether intron-derived dsRNA is released from cells, we immunoprecipitated culture supernatant from KPC cells using the J2 antibody. This showed that intron-derived dsRNA was present in the supernatant of KPC cells and that the amount of dsRNA increased moderately upon depletion of MYC (Figure 6C). To test whether this dsRNA was contained in membranous vesicles, we purified extracellular vesicles by combined filtration and ultracentrifugation and observed a strong enrichment of dsRNA in the vesicle fraction; a mock purification carried out in the presence of a non-ionic detergent, Triton X-100, showed that dsRNA was indeed contained in membranous vesicles (Figure 6D). Consistent with the J2 immunoprecipitation, the amount of dsRNA present in extracellular vesicles increased moderately upon depletion of MYC and this increase was suppressed by expression of MYC, but not by MYCVD (Figure 6D). Incubation of purified extracellular vesicles with

bone marrow-derived dendritic cells confirmed that KPC cells generate extracellular vesicles capable of activating these cells (Supplementary Figure S7F).

To test whether MYC controls the autocrine or paracrine uptake and loading of dsRNA onto TLR3, we immuno-precipitated TLR3 from KPC cells and found that the occupancy of TLR3 with intron-derived dsRNA strongly increased upon depletion of MYC (Figure 6E). Consistently, sgRNA-mediated deletion of MYC in a human PDAC cell line strongly enhanced loading of human repetitive Alu elements onto TLR3 (Supplementary Figure S7G,H). Activation of TLR3 by the synthetic dsRNA, poly (I:C), is sensitive to chloroquine since it requires endosome maturation (29). Consistently, immunoblotting using antibodies against P62/SQSTM1 and LC3 showed a rapid increase in P-P62 levels and LC3-isoform II after depletion of MYC, indicating that depletion of MYC can induce autophagy (Figure 6F). Immunofluorescence experiments showed that TLR3, like the residual dsRNA, re-localized to a perinuclear region when MYC was depleted (Figure 6G). A similar re-localization of TLR3 is observed in response to synthetic dsRNA molecules and has been interpreted as a re-localization to endolysosomes (29). Collectively, our data show that MYC and MIZ1 act at several steps to suppress loading of intron-derived dsRNA onto TLR3 as well as the subsequent traffic of TLR3 to endolysosomes.

TBK1 controls activation of NF-κB and MHC class I gene expression upon depletion of MYC

One well-understood function of TBK1 is the phosphorylation and activation of IRF3, leading to the expression of interferon-dependent genes (31). However, deletion of IRF3 had no effect on the response of KPC tumors to depletion of MYC (Supplementary Figure S8A,B). To clarify the function of TBK1, we compared the effects of MYC depletion in wildtype and TBK1-deficient cells on gene expression by RNA sequencing and found that the induction of NF-κB-dependent genes was significantly attenuated in TBK1-deficient cells (Figure 7A and Supplementary Figure S8C). Furthermore, immunoblots and quantification over several biological replicates using a phospho-specific antibody showed that TBK1 was required for phosphorylation of IκBα upon depletion of MYC (Figure 7B) and expression of a non-phosphorylatable mutant allele of IκBα suppressed induction of NF-κB target genes upon MYC-depletion (Figure 7A). Analysis of the NF-κB dependent genes induced upon MYC depletion showed that they predominantly encode genes involved in inflammatory responses and cell migration (Supplementary Figure 8D). In particular, we observed that multiple MHC class I genes are upregulated upon MYC depletion (Supplementary Figure 8E); this is consistent with previous work demonstrating that MHC class genes are regulated by an NF-kB dependent enhancer element (32). In line with these observations, the expression of H2-K1, and to a lesser degree that of H2-D1, the two major MHC class I genes expressed in these cells, were induced upon MYC depletion in a TBK1- and NF-κB-dependent manner (Figure 7C, Supplementary Figure S8F) (33). In contrast, effects of TBK1 deletion on the expression of multiple cytokines were weak and variable.

To clarify the mode of action of TBK1, we noted that deletion of TBK1 significantly attenuated the expression of many genes involved in endocytosis and autophagosomes formation(Figure 7A). TBK1 can stimulate autophagy via phosphorylation of P62/SQSTM1

(34). Consistent with this finding, deletion of TBK1 clearly attenuated phosphorylation of P62/SQSTM1, suggesting that it attenuates the formation of autophagosomes (Figure 7B). Since activation of TLR3 requires endosome maturation, TBK1 may either act directly to activate NF-κB or indirectly via an effect on endosomal maturation (29). To test whether the decrease in dsRNA observed after MYC depletion depends on lysosomal degradation, we depleted MYC in the presence of increasing concentrations of chloroquine (CQ), which impairs endosome fusion with lysosomes (35). Addition of chloroquine blocked the decrease in dsRNA levels upon MYC depletion in a concentration range that is in line with multiple similar experiments (Supplementary Figure S8G) (35). At the same time, addition of chloroquine moderately enhanced the amount of dsRNA in the supernatant (Supplementary Figure S8H) and strongly enhanced loading of dsRNA onto TLR3 (Figure 7D). Likewise, while deletion of TBK1 had no effect on overall levels of cytosolic dsRNA, it strongly enhanced loading of dsRNA onto TLR3 and abrogated the effect of MYC-depletion on loading, arguing that the transport of TLR3 into endolysosomes is blocked in TBK1-deficient cells (Figure 7E). We concluded that TBK1 is required for activation of NF-κB and most likely acts via its effect on vesicular transport of TLR3 (see graphical abstract). Together with the previous findings, the data argue that a positive feedback loop between TLR3 and TBK1 controls both signaling to NF-κB and degradation of dsRNA.

Discussion

Suppression of pro-inflammatory and NF-κB dependent gene expression by MYC has been observed in multiple experimental systems and closely correlates with the ability of MYC to prevent the recognition of tumors by the immune system (3–5,16,33), hence understanding the underlying molecular mechanisms is of considerable therapeutic interest.

To account for these observations, we propose a model that has two elements: First, we show that PDAC cells contain large amounts of double-stranded RNA, which is derived both from mitochondria and from a group of about 60 nuclear genes, which harbor inverted repetitive elements in their introns that hybridize to form dsRNA. The host genes of intron-derived dsRNA do not encode proteins of a common functional category or respond to a particular stimulus and most likely do not represent a specific gene expression program. Rather, they have very long introns, which is expected to delay the completion of splicing and open a time window for dsRNA formation. In addition, the genes are particularly AT-rich. Since the editing of adenosine to inosine reduces the stability and promotes the subsequent cleavage of dsRNA (36), we propose that degradation of intron-derived dsRNA is limiting in PDAC cells. Collectively, we suggest that these physical features rather than the function of the encoded proteins cause these genes to be sensors for monitoring splicing efficacy. Notably, increased intron retention closely correlates with an extended survival of pancreas carcinoma patients, supporting the concept that intron-derived dsRNA limits tumor growth (37).

The second element of our model is based on the observation that neither MYC nor MIZ1 show significant binding to the promoters of NF-κB regulated genes, arguing that their regulation by MYC is largely indirect. Instead, changes in pro-inflammatory gene expression reflect MYC-dependent changes in the activity of its upstream regulators, TLR3 and TBK1. TBK1 is both activated downstream of TLR3 and controls the transport of

TLR3 to endolysosomes, which activates TLR3, arguing that both proteins act in a positive feedback loop (29). While the effects of MYC on the secretion of dsRNA in extracellular vesicles were moderate, depletion of MYC led to robust increases in loading of intron-derived dsRNA on TLR3, in activation and trafficking of TLR3 and in the subsequent lysosomal degradation of dsRNA. Since MIZ1 binds to a highly conserved set of promoters of multiple genes involved in vesicle transport (18), we suggest that MYC suppresses TBK1 activity and, downstream of TBK1, NF-κB-dependent transcription, via its effect on MIZ1-dependent vesicular traffic. When active, NF-κB promotes the expression of the major MHC class I antigens in response to dsRNA, arguing that it activates T cell function (32). Consistently, our data show that MYC suppresses MHC class I antigens via its effect on the TBK1-NFkB pathway. TBK1 also phosphorylates and activates IRF3, which drives expression of the IFN-α and IFN-β genes (31). Both interferon genes are not expressed in the KPC cells that we studied as well as in multiple murine PDAC cell lines independently established from primary tumors (D. Saur, personal communication), and we were unable to detect phosphorylated IRF3 in these cells, which may be due to the presence of mutant p53 that can interfere with IRF3 phosphorylation by TBK1 (38). Nevertheless, the mechanism we describe could potentially also account for the MIZ1-dependent suppression of interferon-dependent gene expression by MYC (4).

Perturbances in mRNA splicing are a major threat to genomic stability, since they cause accumulation of R-loops and can induce the synthesis of aberrant proteins normally involved in genome maintenance (39). We propose that cells use intron-derived dsRNA to monitor completion of splicing and the absence of R-loops as a means to maintain genomic integrity. This is consistent with previous observations showing that MYC-driven tumor cells are specifically vulnerable to perturbation of mRNA splicing (40,41). Our data here show that MYC and MIZ1 suppress the uptake of dsRNA and thereby control the activity of the TLR3 receptor and its downstream effector, TBK1. Deletion of TBK1 alleviates the dependence of PDAC tumor growth on MYC, demonstrating that limiting TBK1 activity is the critical function of MYC in this model. Together with the observation that the critical cargo in this pathway is dsRNA, these findings open new avenues to overcome MYC-mediated immune evasion. For example, the enzymes that control the transport and stability of dsRNA and thereby limit its accumulation may be valid targets to achieve this (30). Furthermore, interfering with co-transcriptional splicing can promote the production of immunogenic dsRNA (42) suggesting that inhibition of splicing may also overcome immune evasion.

Supplementary Material

Refer to Web version on PubMed Central for supplementary material.

Acknowledgements

We thank Jens Siveke (Technical University of Munich) for providing KPC cells. We thank Annalena Fischer, Barbara Bauer, Ulrike Samfaß, Ryan Ramjan, Tobias Roth and Sarah Hess for technical support. This work was supported by grants from the German Research Foundation via the DFG Research Group 2314 (“Targeting Therapeutic Windows in essential cellular processes for tumor therapy”) to M.Eilers and L.Zender, the iFIT Cluster of Excellence EXC 2180 “Image Guided and Functionally Instructed Tumor Therapies” to L.Zender and from the European Research Council (AUROMYC) to M.Eilers.

Europe PMC Funders Author Manuscripts

Data availability

RNA-, 4sU- and double-stranded RNA- sequencing datasets are deposited at the GEO (Gene Expression Omnibus) database (RRID:SCR_005012) under the GEO accession number: GSE154903.

References

1. Dang CV. MYC on the path to cancer. Cell. 2012; 149 :22–35. [PubMed: 22464321]
2. Baluapuri A, Wolf E, Eilers M. Target gene-independent functions of MYC oncoproteins. Nature reviews. 2020; 21 :255–67.
3. Topper MJ, Vaz M, Chiappinelli KB, DeStefano Shields CE, Niknafs N, Yen RC, et al. Epigenetic Therapy Ties MYC Depletion to Reversing Immune Evasion and Treating Lung Cancer. Cell. 2017; 171 :1284–300. e21 [PubMed: 29195073]
4. Muthalagu N, Monteverde T, Raffo-Iraolagoitia X, Wiesheu R, Whyte D, Hedley A, et al. Repression of the Type I Interferon pathway underlies MYC & KRAS-dependent evasion of NK & B cells in Pancreatic Ductal Adenocarcinoma. Cancer Discov. 2020
5. Kortlever RM, Sodir NM, Wilson CH, Burkhart DL, Pellegrinet L, Brown Swigart L, et al. Myc Cooperates with Ras by Programming Inflammation and Immune Suppression. Cell. 2017; 171 :1301–15. e14 [PubMed: 29195074]
6. Casey SC, Tong L, Li Y, Do R, Walz S, Fitzgerald KN, et al. MYC regulates the antitumor immune response through CD47 and PD-L1. Science. 2016; 352 :227–31. [PubMed: 26966191]
7. Swaminathan S, Hansen AS, Heftdal LD, Dhanasekaran R, Deutzmann A, Fernandez WDM, et al. MYC functions as a switch for natural killer cell-mediated immune surveillance of lymphoid malignancies. Nat Commun. 2020; 11 :2860. [PubMed: 32503978]
8. Taniguchi K, Karin M. NF-kappaB, inflammation, immunity and cancer: coming of age. Nature reviews Immunology. 2018; 18 :309–24.
9. Brubaker SW, Bonham KS, Zanoni I, Kagan JC. Innate immune pattern recognition: a cell biological perspective. Annu Rev Immunol. 2015; 33 :257–90. [PubMed: 25581309]
10. Chow KT, Gale M Jr, Loo YM. RIG-I and Other RNA Sensors in Antiviral Immunity. Annu Rev Immunol. 2018; 36 :667–94. [PubMed: 29677479]
11. Kwon J, Bakhoum SF. The Cytosolic DNA-Sensing cGAS-STING Pathway in Cancer. Cancer Discov. 2020; 10 :26–39. [PubMed: 31852718]
12. Mackenzie KJ, Carroll P, Martin CA, Murina O, Fluteau A, Simpson DJ, et al. cGAS surveillance of micronuclei links genome instability to innate immunity. Nature. 2017; 548 :461–5. [PubMed: 28738408]
13. West AP, Khoury-Hanold W, Staron M, Tal MC, Pineda CM, Lang SM, et al. Mitochondrial DNA stress primes the antiviral innate immune response. Nature. 2015; 520 :553–7. [PubMed: 25642965]
14. Vaseva AV, Blake DR, Gilbert TSK, Ng S, Hostetter G, Azam SH, et al. KRAS Suppression-Induced Degradation of MYC Is Antagonized by a MEK5-ERK5 Compensatory Mechanism. Cancer cell. 2018; 34 :807–22. e7 [PubMed: 30423298]
15. Walz S, Lorenzin F, Morton J, Wiese KE, von Eyss B, Herold S, et al. Activation and repression by oncogenic MYC shape tumour-specific gene expression profiles. Nature. 2014; 511 :483–7. [PubMed: 25043018]
16. Sodir NM, Kortlever RM, Barthet VJA, Campos T, Pellegrinet L, Kupczak S, et al. MYC Instructs and Maintains Pancreatic Adenocarcinoma Phenotype. Cancer Discov. 2020
17. Wiese KE, Walz S, von Eyss B, Wolf E, Athineos D, Sansom O, et al. The role of MIZ-1 in MYC-dependent tumorigenesis. Cold Spring Harbor perspectives in medicine. 2013; 3 a014290 [PubMed: 24296348]
18. Wolf E, Gebhardt A, Kawauchi D, Walz S, von Eyss B, Wagner N, et al. Miz1 is required to maintain autophagic flux. Nat Commun. 2013; 4 :2535. [PubMed: 24088869]

19. Kim Y, Park J, Kim S, Kim M, Kang MG, Kwak C, et al. PKR Senses Nuclear and Mitochondrial Signals by Interacting with Endogenous Double-Stranded RNAs. Mol Cell. 2018; 71 :1051–63. e6 [PubMed: 30174290]
20. Dhir A, Dhir S, Borowski LS, Jimenez L, Teitell M, Rotig A, et al. Mitochondrial double-stranded RNA triggers antiviral signalling in humans. Nature. 2018; 560 :238–42. [PubMed: 30046113]
21. Witkiewicz AK, McMillan EA, Balaji U, Baek G, Lin WC, Mansour J, et al. Whole-exome sequencing of pancreatic cancer defines genetic diversity and therapeutic targets. Nat Commun. 2015; 6 :6744. [PubMed: 25855536]
22. Hingorani SR, Wang L, Multani AS, Combs C, Deramaudt TB, Hruban RH, et al. Trp53R172H and KrasG12D cooperate to promote chromosomal instability and widely metastatic pancreatic ductal adenocarcinoma in mice. Cancer cell. 2005; 7 :469–83. [PubMed: 15894267]
23. Pearson T, Shultz LD, Miller D, King M, Laning J, Fodor W, et al. Non-obese diabetic-recombination activating gene-1 (NOD-Rag1 null) interleukin (IL)-2 receptor common gamma chain (IL2r gamma null) null mice: a radioresistant model for human lymphohaematopoietic engraftment. Clin Exp Immunol. 2008; 154 :270–84. [PubMed: 18785974]
24. Skourti-Stathaki K, Kamieniarz-Gdula K, Proudfoot NJ. R-loops induce repressive chromatin marks over mammalian gene terminators. Nature. 2014; 516 :436–9. [PubMed: 25296254]
25. Li F, Wang Y, Zeller KI, Potter JJ, Wonsey DR, O'Donnell KA, et al. Myc stimulates nuclearly encoded mitochondrial genes and mitochondrial biogenesis. Mol Cell Biol. 2005; 25 :6225–34. [PubMed: 15988031]
26. Leonard JN, Ghirlando R, Askins J, Bell JK, Margulies DH, Davies DR, et al. The TLR3 signaling complex forms by cooperative receptor dimerization. Proceedings of the National Academy of Sciences of the United States of America. 2008; 105 :258–63. [PubMed: 18172197]
27. Brisse M, Ly H. Comparative Structure and Function Analysis of the RIG-I-Like Receptors: RIG-I and MDA5. Frontiers in immunology. 2019; 10 :1586. [PubMed: 31379819]
28. Cheng K, Wang X, Yin H. Small-molecule inhibitors of the TLR3/dsRNA complex. J Am Chem Soc. 2011; 133 :3764–7. [PubMed: 21355588]
29. Lee HK, Dunzendorfer S, Soldau K, Tobias PS. Double-stranded RNA-mediated TLR3 activation is enhanced by CD14. Immunity. 2006; 24 :153–63. [PubMed: 16473828]
30. Ishizuka JJ, Manguso RT, Cheruiyot CK, Bi K, Panda A, Iracheta-Vellve A, et al. Loss of ADAR1 in tumours overcomes resistance to immune checkpoint blockade. Nature. 2019; 565 :43–8. [PubMed: 30559380]
31. Fitzgerald KA, McWhirter SM, Faia KL, Rowe DC, Latz E, Golenbock DT, et al. IKKepsilon and TBK1 are essential components of the IRF3 signaling pathway. Nature immunology. 2003; 4 :491–6. [PubMed: 12692549]
32. Dhatchinamoorthy K, Colbert JD, Rock KL. Cancer Immune Evasion Through Loss of MHC Class I Antigen Presentation. Frontiers in immunology. 2021; 12 636568 [PubMed: 33767702]
33. Versteeg R, Noordermeer IA, Kruse-Wolters M, Ruiter DJ, Schrier PI. c-myc down-regulates class I HLA expression in human melanomas. The EMBO journal. 1988; 7 :1023–9. [PubMed: 3402430]
34. Matsumoto G, Shimogori T, Hattori N, Nukina N. TBK1 controls autophagosomal engulfment of polyubiquitinated mitochondria through p62/SQSTM1 phosphorylation. Hum Mol Genet. 2015; 24 :4429–42. [PubMed: 25972374]
35. Mauthe M, Orhon I, Rocchi C, Zhou X, Luhr M, Hijlkema KJ, et al. Chloroquine inhibits autophagic flux by decreasing autophagosome-lysosome fusion. Autophagy. 2018; 14 :1435–55. [PubMed: 29940786]
36. Nishikura K. A-to-I editing of coding and non-coding RNAs by ADARs. Nature reviews. 2016; 17 :83–96.
37. Tan DJ, Mitra M, Chiu AM, Coller HA. Intron retention is a robust marker of intertumoral heterogeneity in pancreatic ductal adenocarcinoma. NPJ Genom Med. 2020; 5 :55. [PubMed: 33311498]
38. Ghosh M, Saha S, Bettke J, Nagar R, Parrales A, Iwakuma T, et al. Mutant p53 suppresses innate immune signaling to promote tumorigenesis. Cancer cell. 2021; 39 :494–508. e5 [PubMed: 33545063]

39. Tam AS, Stirling PC. Splicing, genome stability and disease: splice like your genome depends on it! Curr Genet. 2019; 65 :905–12. [PubMed: 30953124]

40. Hsu TY, Simon LM, Neill NJ, Marcotte R, Sayad A, Bland CS, et al. The spliceosome is a therapeutic vulnerability in MYC-driven cancer. Nature. 2015; 525 :384–8. [PubMed: 26331541]

41. Cossa G, Roeschert I, Prinz F, Baluapuri A, Silveira Vidal R, Schulein-Volk C, et al. Localized Inhibition of Protein Phosphatase 1 by NUAK1 Promotes Spliceosome Activity and Reveals a MYC-Sensitive Feedback Control of Transcription. Mol Cell. 2020; 77 :1322–39. e11 [PubMed: 32006464]

42. Bowling EA, Wang JH, Gong F, Wu W, Neill NJ, Kim IS, et al. Spliceosome-targeted therapies trigger an antiviral immune response in triple-negative breast cancer. Cell. 2021; 184 :384–403. e21 [PubMed: 33450205]

Europe PMC Funders Author Manuscripts

Europe PMC Funders Author Manuscripts

Statement of Significance

This study identifies a TBK1-dependent pathway that links dsRNA metabolism to anti-tumor immunity and shows that suppression of TBK1 is a critical function of MYC in pancreatic ductal adenocarcinoma.

Europe PMC Funders Author Manuscripts

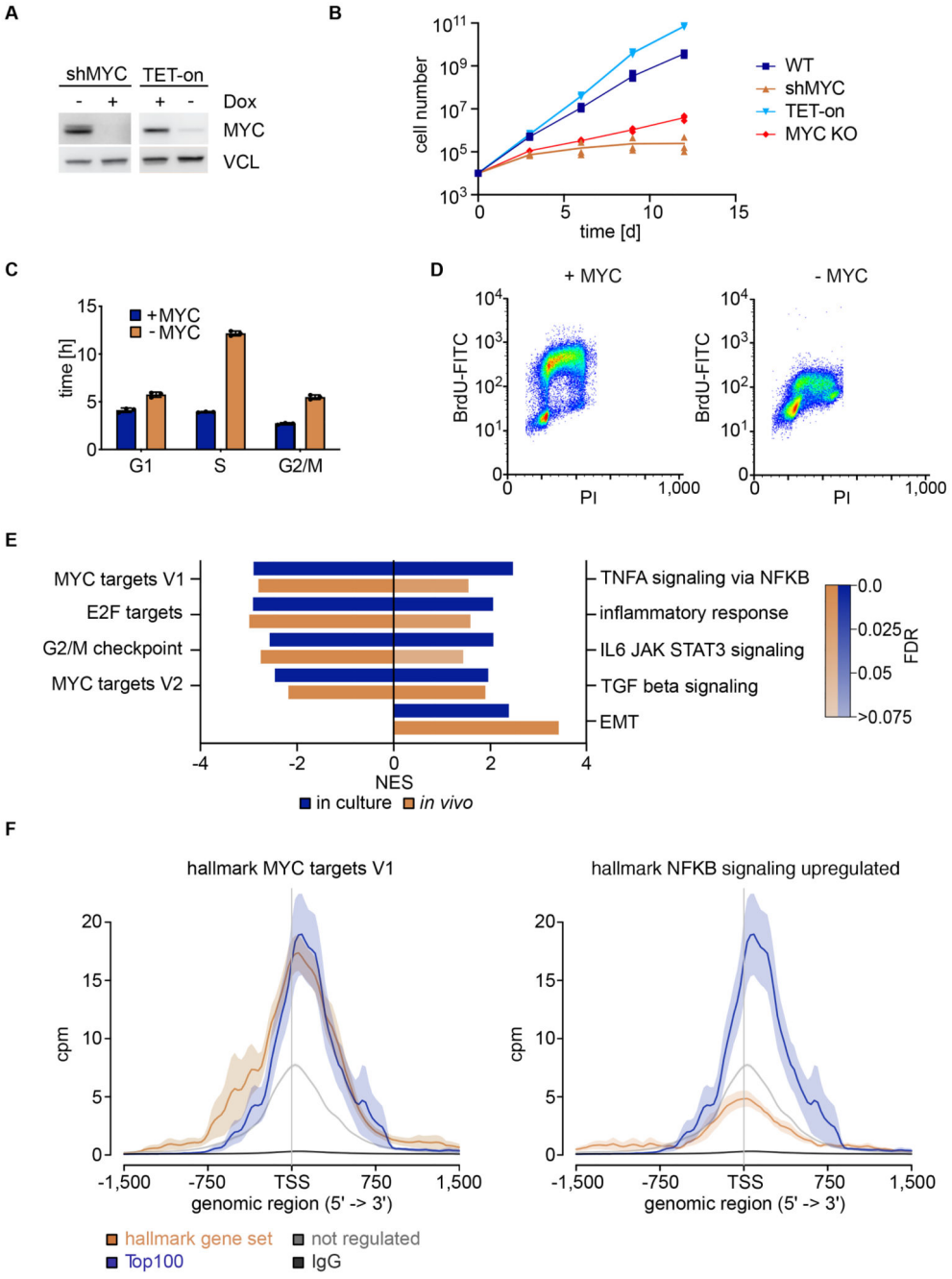

Figure 1. MYC is required for the rapid growth of murine PDAC cells in culture.

A. Immunoblot of KPC cells expressing doxycycline-inducible shRNA targeting MYC (left) and cells in which endogenous MYC has been deleted and which express a doxycycline-inducible (TET-on) human MYC-transgene (right). Where indicated, 1 μg/mL doxycycline was added for 48 h (n=5; in all subsequent legends, n indicates the number of independent biological replicates).

B. Cumulative growth curve of KPC with depletion (shMYC) or deletion of MYC (MYC KO) cells (n=3).

C.Duration of cell cycle calculated from doubling time and cell cycle analysis. Results are presented as individual values +/- S.D. (standard deviation) (n=3).
D.Propidium-iodide (PI) and BrdU FACS-profile of KPC cells expressing doxycycline-inducible shMYC. To deplete MYC, doxycycline was added for 48 h (n=1).
E.Gene set-enrichment analysis of RNA sequencing of KPC cells expressing doxycycline-inducible shMYC in culture (n=3) and samples derived from tumors (n=5) of orthotopically transplanted KPC cells after 48 h doxycycline treatment. A selection of significantly down- or up-regulated hallmark gene sets is shown.
F.Metagene of ChIP sequencing experiment KPC cells comparing MYC binding to different gene sets. Counts per millions (cpm) are plotted. Top100 are the 100 most strongly activated genes from the RNA sequencing experiment; not regulated genes are 100 highly expressed genes that do not change expression in response to MYC depletion. The orange line indicates MYC-binding at selected hallmark gene set. Shadow shows S.E.M. (standard error of the mean) (n=1).

Europe PMC Funders Author Manuscripts

Europe PMC Funders Author Manuscripts

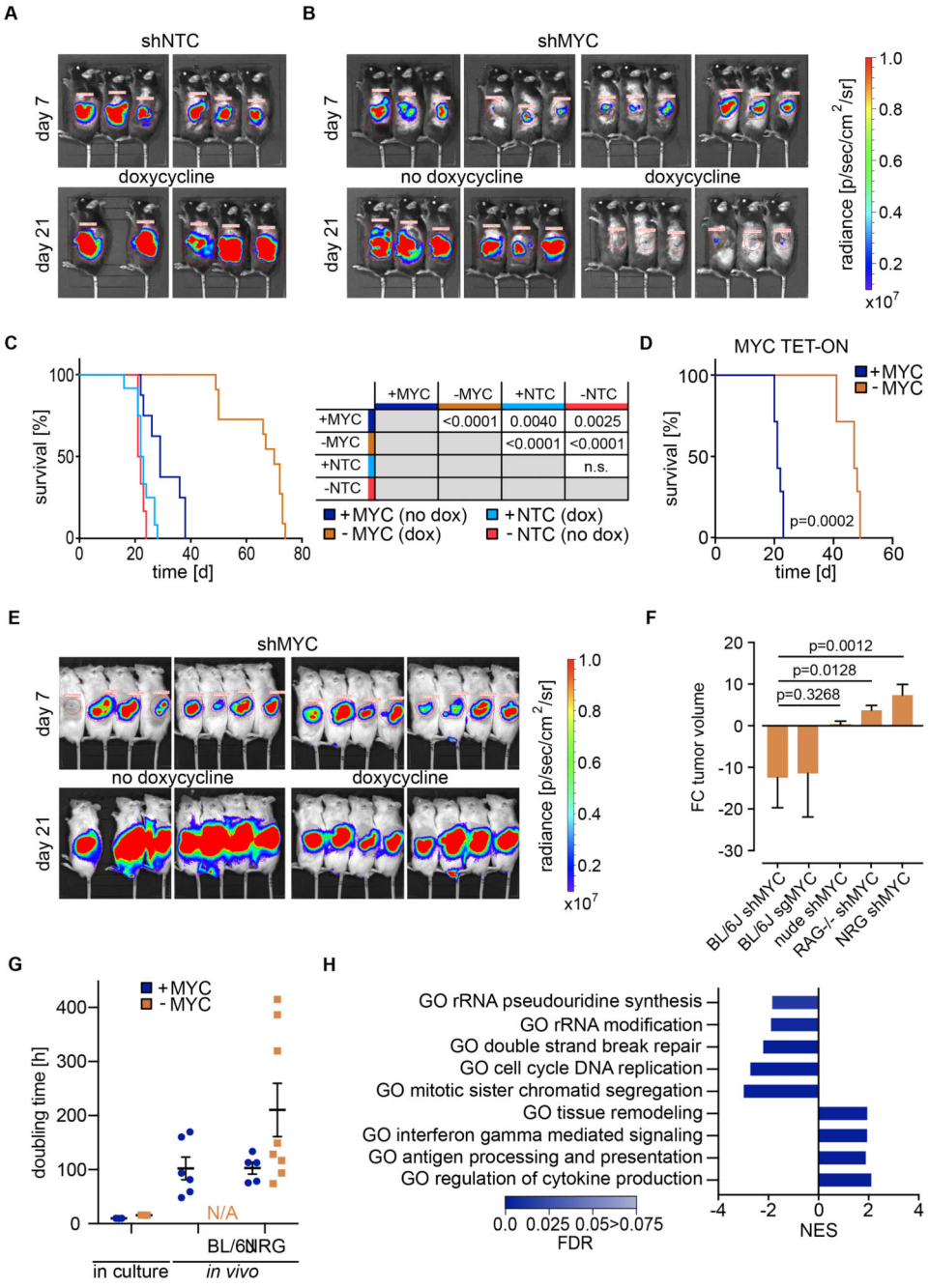

Figure 2. Tumor regression upon MYC depletion is dependent on the immune system.

A. Luciferase imaging of KPC-cell-derived tumors expressing NTC (non-targeting control) shRNA upon orthotopic transplantation into C57BL/6J mice. Doxycycline treatment was started 7 days after transplantation. Luciferase activity of KPC cells measured at 7 days and 21 days after orthotopic transplantation.

B. Luciferase imaging of KPC-cell-derived tumors expressing inducible shMYC in C57BL/6J mice. Experiment was carried out as described in A.

C. Left: Kaplan-Meier plot of mice transplanted with KPC cells expressing doxycycline-inducible shMYC or non-targeting control (NTC). Expression of shRNAs was induced with doxycycline. Right: P values were calculated using Mantel-Cox Test. (n=6 (NTC, no Dox), n=12 (NTC, Dox), n=8 (+MYC, no Dox) and n=11 (-MYC, Dox)).

D. Kaplan-Meier plot of mice transplanted with KPC cells with knockout of the endogenous MYC and doxycycline-induced expression of a MYC-transgene (p=0.0002) (n=7 for each group). P value were calculated using Mantel-Cox Test.

E. Luciferase imaging of KPC-cell-derived tumors expressing doxycycline-inducible shRNAs targeting MYC upon orthotopic transplantation into NRG mice. Doxycycline treatment was started 7 days after transplantation. Luciferase activity of KPC cells was measured after 7 and 21 days after orthotopic transplantation (n=8 for each arm).

F. Change of tumor volume measured with IVIS upon depletion or deletion of MYC of over 14 days treatment after transplantation and engraftment of KPC cells expressing inducible shMYC. Cells were transplanted in C57BL/6J, nude, RAG1$^{-/-}$ mice or NRG mice as indicated. KPC cells with knockout of MYC were also transplanted into C57BL/6J mice. Results are presented as mean +/- S.E.M.

G. Estimated doubling time of KPC cells in culture (n=3) and *in vivo* (n=6 (B6/J), n=5 (NRG, +MYC) and n=8 (NRG, -MYC)) upon depletion of MYC. Results are presented as individual values +/- S.E.M.

H. GO term analysis of differentially expressed genes between tumor tissue 9 days after implantation and tumor cells in culture, both treated for 48h with doxycyclin.

Europe PMC Funders Author Manuscripts

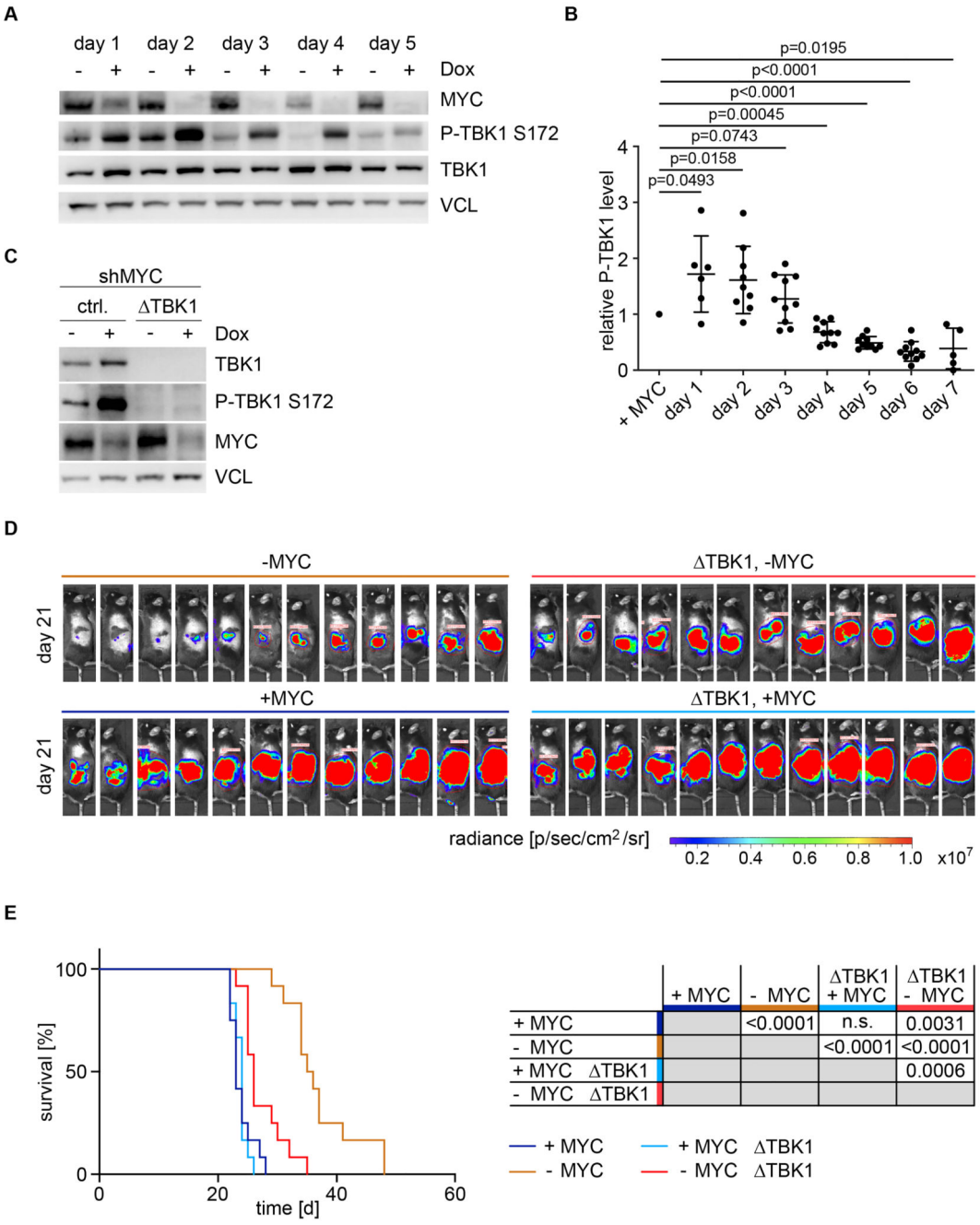

Figure 3. Activation of TBK1 is critical for tumor regression upon MYC depletion.

A. Immunoblot of MYC, TBK1 and P-TBK1 of KPC cells expressing doxycycline-inducible shRNAs targeting MYC after the indicated times of doxycycline addition (n=7).

B. Quantification of immunoblot for P-TBK1 over 7 days. Results are presented as individual values +/- S.D. P values were calculated using two-tailed t-test comparing +MYC to every single time point with MYC depletion.

C. Immunoblot of KPC cells comparing response of wildtype KPC cells and those with CRISPR/Cas9 mediated deletion of TBK1 to doxycycline-induced depletion of MYC for 48 h (n=3).

D. Luciferase imaging of control and TBK1-deleted KPC-cell-derived tumors expressing shMYC upon orthotopic transplantation into C57BL/6J mice after 21 days. Doxycycline treatment was started 7 days after transplantation (n=12 for each group).

E. Left: Kaplan-Meier plot of mice transplanted with KPC cells without or with knockout of TBK1 and doxycycline-inducible expression of shMYC (n=12 for each group). Right: P values calculated with Mantel-Cox test.

Europe PMC Funders Author Manuscripts

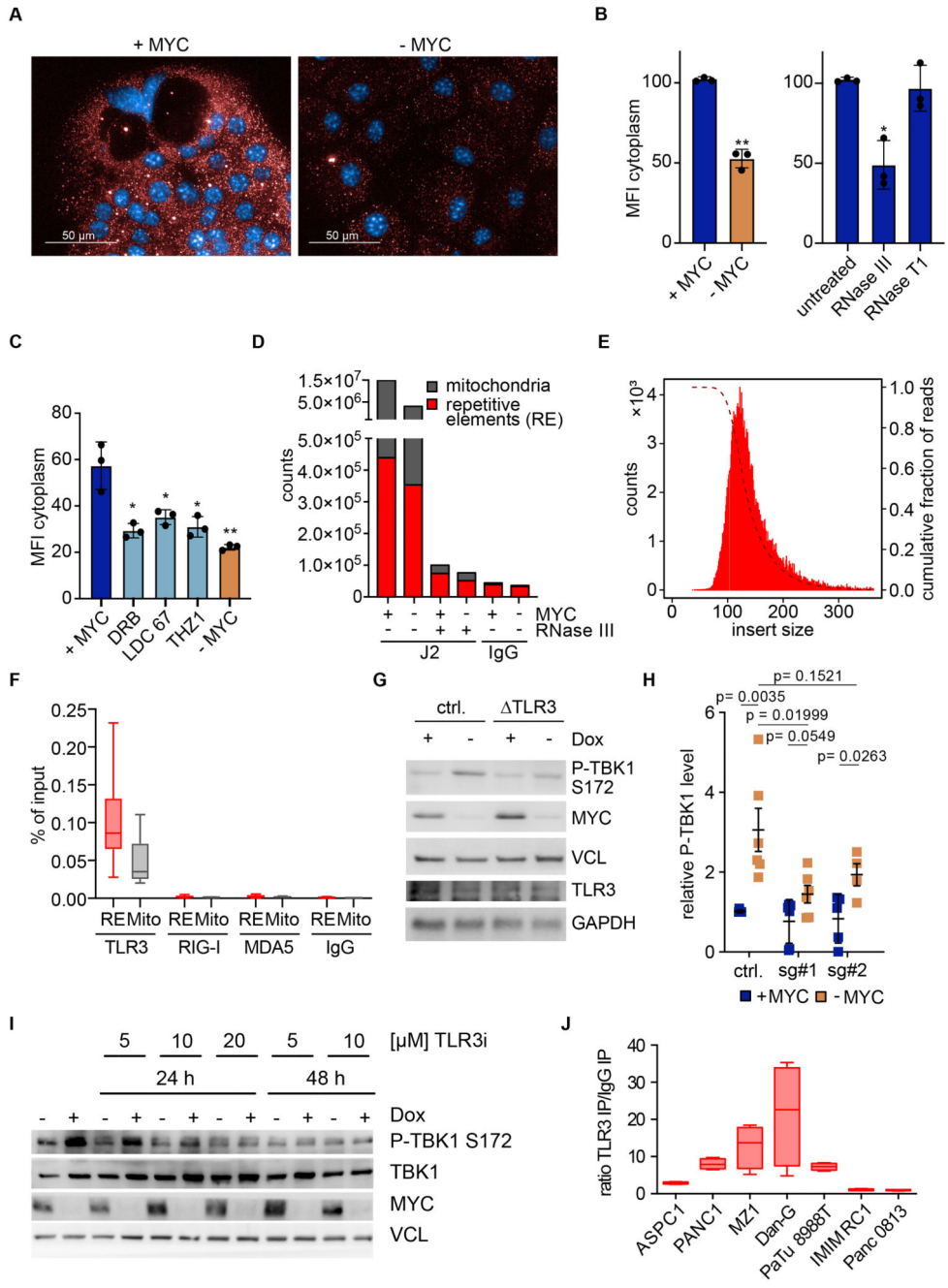

Figure 4. dsRNA-mediated activation of TBK1 in KPC cells.

A. Immunofluorescence of dsRNA (J2) in KPC cells before and after 48 h of MYC depletion using inducible shMYC. Nuclei were stained using Hoechst (n=3).

B. Mean fluorescent intensity (MFI) of dsRNA-signal in the cytoplasm of the KPC cells after MYC depletion (p=0.0039, two-tailed t-test). Treatment with RNase T1 or RNase III (p=0.0272, two-tailed t-test) treatment were used as control (n=3).

C. Quantification of immunofluorescence for dsRNA in the cytoplasm of the KPC cells upon depletion of MYC or inhibition of CDK9 (DRB 25 μM; LDC 0000 67 100 μM) or CDK7 (THZ1, 200 nM) for 24 h. P value was calculated using two-tailed t-test (n=3).

D. Spike-normalized sequencing of J2 immunoprecipitates. Plot shows distribution of reads located on the mitochondrial chromosome and repetitive elements (nuclear origin). RNase III and IgG were included as control (n=1).

E. Length distribution of dsRNA-reads originating in the nucleus. Dashed line represents cumulative distribution.

F. fCLIP performed in untreated KPC cells with antibodies against TLR3, RIG-I, MDA5 and IgG as control. Box plot shows different primers from RQ-PCR grouped according origin of dsRNA +/- S.D. (n=2). RE: primer target sequence from nuclear repetitive elements, Mito: primer target sequence of mitochondrial dsRNA.

G. Immunoblot of in KPC cells with a CRISPR/Cas9 mediated deletion of TLR3, inducible expression of MYC and knockout of endogenous MYC (n=6).

H. Quantification of TBK1 phosphorylation upon TLR3 deletion using two different sgRNAs. Results are presented as individual values +/- S.E.M. P value was calculated using two-tailed t-test.

I. Immunoblots documenting phosphorylation of TBK1 after MYC depletion upon pre-incubation of cells with the indicated concentrations of (*R*)-2-(3-Chloro-6-fluorobenzo[b]thiophene-2-carboxamido)-3-phenylpropanoic acid (TLR3i) (28).

J. fCLIP performed in human PDAC cell lines against TLR3. Box plot show average ratio of dsRNA present in TLR3 relative control IP using different primers +/- S.D. (n=2).

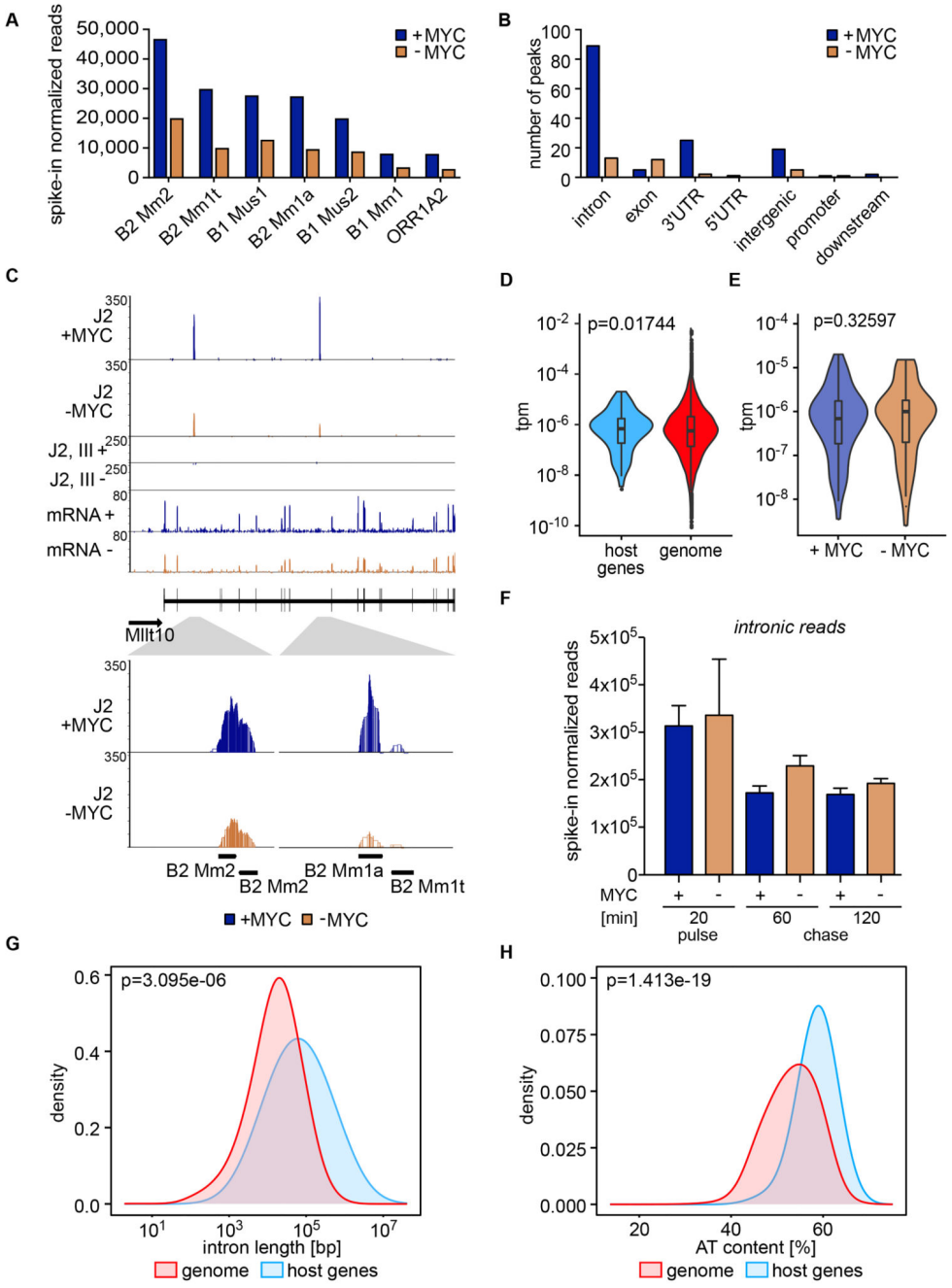

Figure 5. Double-stranded RNA derives from inverted repetitive elements in the nucleus.

A. Spike-in-normalized reads located on repetitive elements in the nuclear genome ranked according to expression level and selected for MYC regulated fold change (FC).”+MYC” indicates rescue of MYC expression from a doxycycline inducible transgene, “-MYC” indicates CRISPR/Cas9 mediated knockout of MYC without expression of MYC from transgene for 48 h (n=1).

B. Location of dsRNA peaks in the nuclear genome derived from sequencing of J2 immunoprecipitates.

C. Exemplary browser track of dsRNA peaks in intron of *Mllt10* gene derived from deep sequencing of dsRNA.
D. Comparison of expression of genes with dsRNA peaks (“host genes”) compared to all expressed genes. Transcripts per kilobase million (tpm) are plotted.
E. Comparison of the expression of host genes in “+ MYC” and “-MYC” conditions. Transcripts per kilobase million (tpm) are plotted.
F. Intronic reads from host genes of dsRNA obtained after labeling of nascent RNA using 4-thiouridine for 20 min and a chase for 60 and 120 min as indicated in KPC cells with and without depletion of MYC for 48 h. Results are presented as mean +/- S.E.M (n=3).
G. Density plot of the total intron length of genes (sum of all introns) with a dsRNA peak within their intron versus all murine genes.
H. Density plot of the AT content of genes with a dsRNA peak within their intron versus all murine genes.

Europe PMC Funders Author Manuscripts

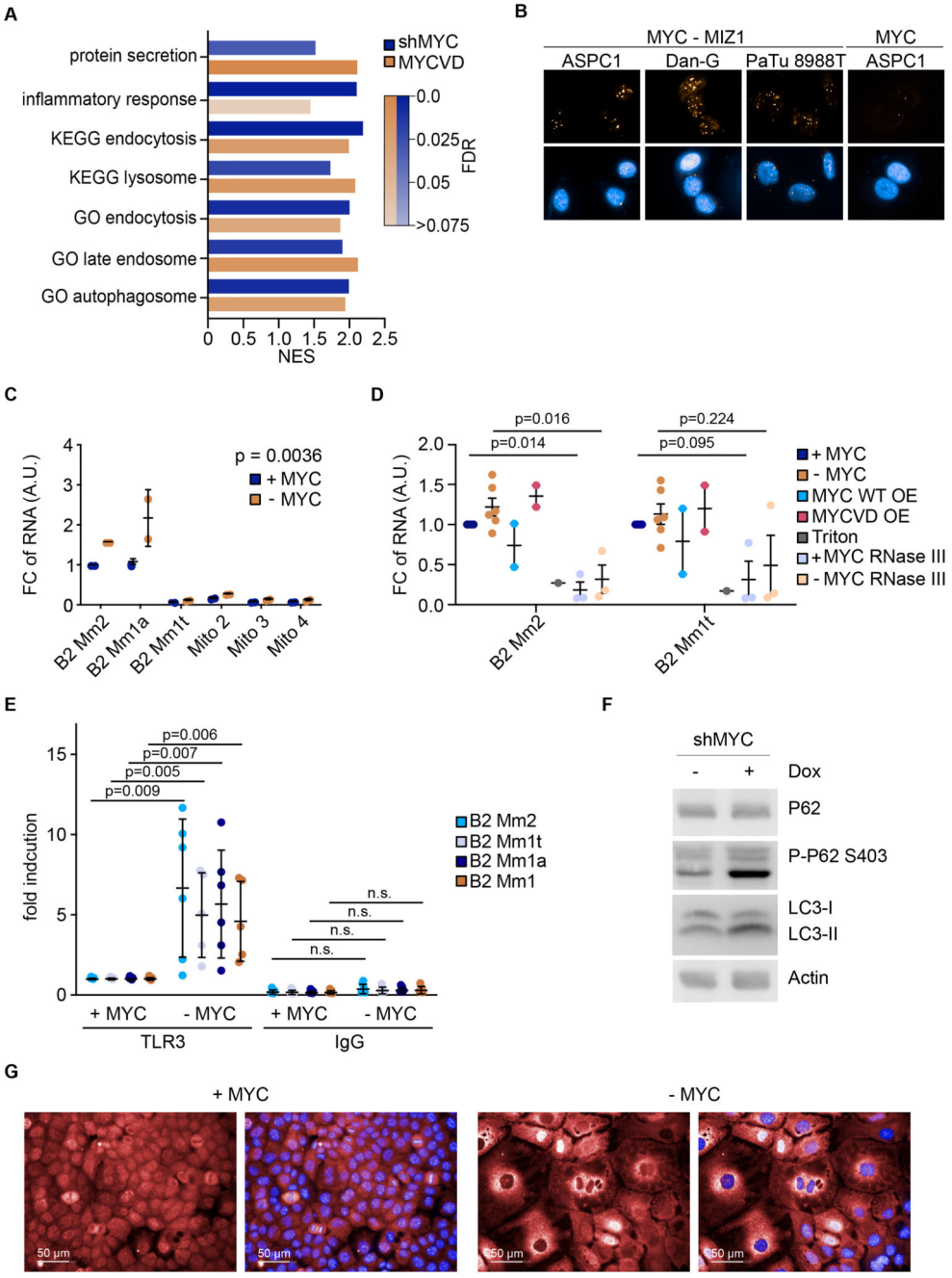

Figure 6. MYC and MIZ control trafficking of dsRNA

A. Comparison of gene set enrichment analysis (GSEA) of KPC cells with wildtype levels of MYC and shRNA mediated MYC depletion after 48 h (left column) and ectopic expression of mutant MYCVD compared to expression of wildtype MYC for 48 h (right column)(n=3). Significantly upregulated hallmark gene sets and GO terms are shown with indicated NES and FDR.

B. Proximity ligation assay of MYC and MIZ1 in human PDAC cell lines (n=3).

Europe PMC Funders Author Manuscripts

C. RQ-PCR of immunoprecipitates with J2 antibody from supernatant of KPC cells. Results are presented as individual values (n=2). P value was calculated using 2-way RM ANOVA.
D. Purification of extracellular vesicles from the supernatant of KPC cells followed by RNA-extraction and RQ-PCR (n=6). Results are presented as mean +/- S.E.M. P value was calculated using 2-tailed, unpaired t-test.
E. fCLIP from KPC cells and KPC cells with shRNA mediated MYC depletion after 48 h. Precipitation was done with anti-TLR3 and IgG as control. Results are presented as mean +/- S.E.M. P value was calculated using 2-tailed, unpaired t-test (n=6).
F. Immunoblot for P62 and P-P62 (S403) and LC3 upon depletion of MYC using inducible shRNAs (n=3).
G. Immunofluorescence of TLR3 in KPC cells and KPC cells upon MYC depletion. Nuclei were stained using Hoechst (n=2).

Europe PMC Funders Author Manuscripts

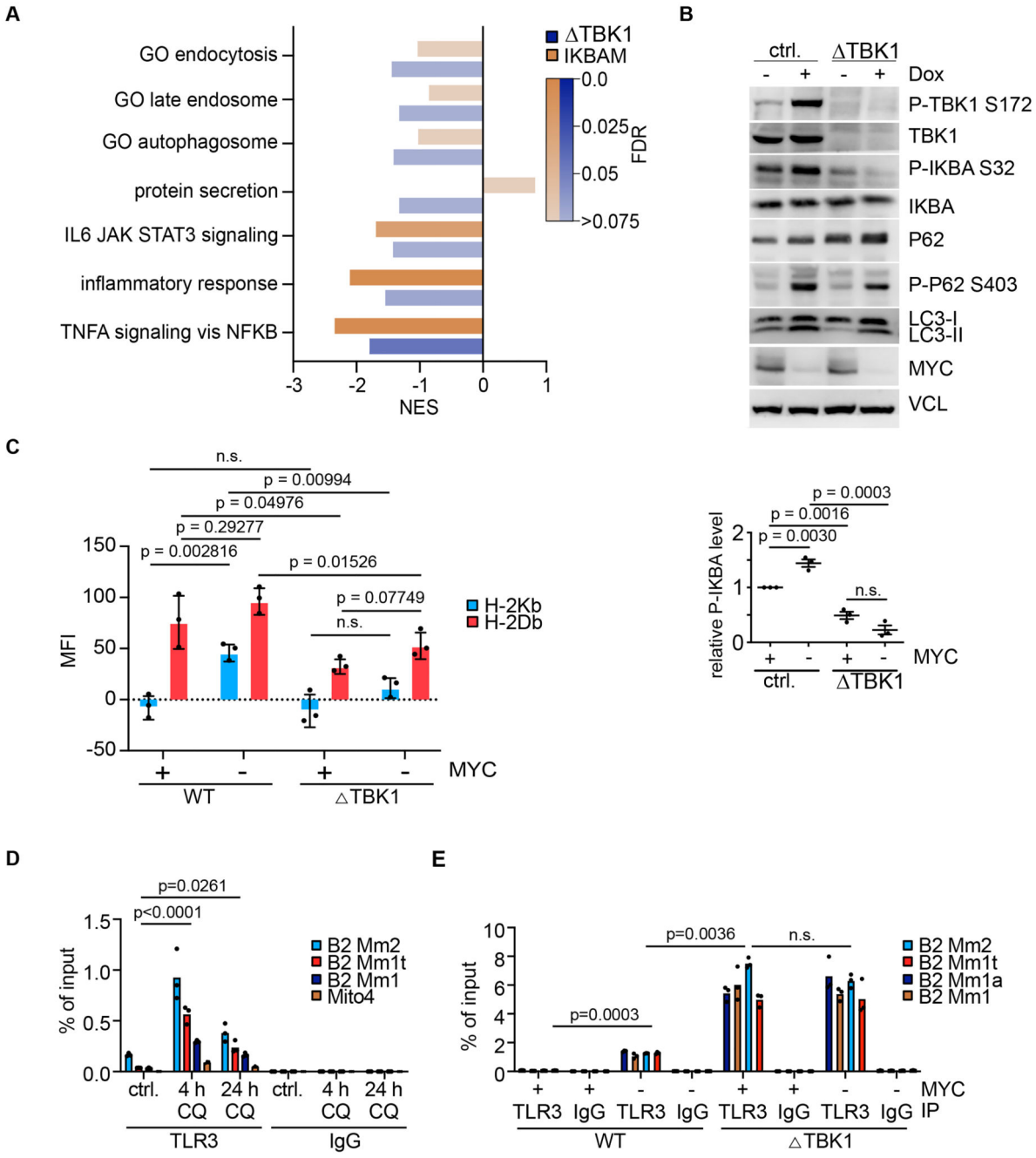

Figure 7. TBK1 controls activation of NF-κB upon depletion of MYC

A. GSEA of global expression analysis from KPC cells with knockout of TBK1 and wildtype TBK1 or overexpression of a non-phosphorylatable IκBα mutant, both with shRNA mediated depletion of MYC (n=3). Significantly downregulated hallmark gene sets and GO terms are shown.

B. (Top) Immunoblot of indicated proteins upon shRNA mediated depletion of MYC and knockout of TBK1 (Bottom): Quantification of P-IκBα signal. Results are presented as biological replicates +/- S.D. P value was calculated using 2-tailed, unpaired t-test (n=3).

Europe PMC Funders Author Manuscripts

C. FACS analysis of H2-K1 and H2-D1 cell surface expression under the indicated experimental conditions. Data is presented as individual values of biological replicates and mean +/- S.D. (n=3). P values were calculated using One-Way-Anova with post Hoc Tukey.
D. fCLIP from KPC cells treated with 10 μM Chloroquine (CQ) for 4 h or 24 h (n=2). P value was calculated using ANOVA with Fisher's LSD.
E. fCLIP from KPC cells with inducible MYC depletion and knockout of TBK1 compared to wildtype TBK1. Results are presented as individual values of technical replicates (n=2). P value was calculated using ANOVA with Fisher's LSD.

Europe PMC Funders Author Manuscripts